

First measurement of near-threshold J/ψ exclusive photoproduction off the proton

A. Ali,¹⁰ M. Amarian,²² E. G. Anassontzis,² A. Austregesilo,³ M. Baalouch,²² F. Barbosa,¹⁴ J. Barlow,⁷ A. Barnes,³ E. Barriga,⁷ T. D. Beattie,²³ V. V. Berdnikov,¹⁷ T. Black,²⁰ W. Boeglin,⁶ M. Boer,⁴ W. J. Briscoe,⁸ T. Britton,¹⁴ W. K. Brooks,²⁴ B. E. Cannon,⁷ N. Cao,¹¹ E. Chudakov,¹⁴ S. Cole,¹ O. Cortes,⁸ V. Crede,⁷ M. M. Dalton,¹⁴ T. Daniels,²⁰ A. Deur,¹⁴ S. Dobbs,⁷ A. Dolgolenko,¹³ R. Dotel,⁶ M. Dugger,¹ R. Dzhygadlo,¹⁰ H. Egiyan,¹⁴ A. Ernst,⁷ P. Eugenio,⁷ C. Fanelli,¹⁶ S. Fegan,⁸ A. M. Foda,²³ J. Foote,¹² J. Frye,¹² S. Furlotov,¹⁴ L. Gan,²⁰ A. Gasparian,¹⁹ V. Gauzshtein,^{25,26} N. Gevorgyan,²⁷ C. Gleason,¹² K. Goetzen,¹⁰ A. Goncalves,⁷ V. S. Goryachev,¹³ L. Guo,⁶ H. Hakobyan,²⁴ A. Hamdi,¹⁰ S. Han,²⁹ J. Hardin,¹⁶ G. M. Huber,²³ A. Hurley,²⁸ D. G. Ireland,⁹ M. M. Ito,¹⁴ N. S. Jarvis,³ R. T. Jones,⁵ V. Kakoyan,²⁷ G. Kalicy,⁴ M. Kamel,⁶ C. Kourkoumelis,² S. Kuleshov,²⁴ I. Kuznetsov,^{25,26} I. Larin,¹⁵ D. Lawrence,¹⁴ D. I. Lersch,⁷ H. Li,³ W. Li,²⁸ B. Liu,¹¹ K. Livingston,⁹ G. J. Lolos,²³ V. Lyubovitskij,^{25,26} D. Mack,¹⁴ H. Marukyan,²⁷ V. Matveev,¹³ M. McCaughan,¹⁴ M. McCracken,³ W. McGinley,³ J. McIntyre,⁵ C. A. Meyer,³ R. Miskimen,¹⁵ R. E. Mitchell,¹² F. Mokaya,⁵ F. Nerling,¹⁰ L. Ng,⁷ A. I. Ostrovidov,⁷ Z. Papandreou,²³ M. Patsyuk,¹⁶ P. Pauli,⁹ R. Pedroni,¹⁹ L. Pentchev,^{14,*} K. J. Peters,¹⁰ W. Phelps,⁸ E. Pooser,¹⁴ N. Qin,²¹ J. Reinhold,⁶ B. G. Ritchie,¹ L. Robison,²¹ D. Romanov,¹⁷ C. Romero,²⁴ C. Salgado,¹⁸ A. M. Schertz,²⁸ R. A. Schumacher,³ J. Schwiening,¹⁰ K. K. Seth,²¹ X. Shen,¹¹ M. R. Shepherd,¹² E. S. Smith,¹⁴ D. I. Sober,⁴ A. Somov,¹⁴ S. Somov,¹⁷ O. Soto,²⁴ J. R. Stevens,²⁸ I. I. Strakovsky,⁸ K. Suresh,²³ V. Tarasov,¹³ S. Taylor,¹⁴ A. Teymurazyan,²³ A. Thiel,⁹ G. Vasileiadis,² D. Werthmüller,⁹ T. Whitlatch,¹⁴ N. Wickramaarachchi,²² M. Williams,¹⁶ T. Xiao,²¹ Y. Yang,¹⁶ J. Zarling,¹² Z. Zhang,²⁹ G. Zhao,¹¹ Q. Zhou,¹¹ X. Zhou,²⁹ and B. Zihlmann¹⁴

(The GLUEX Collaboration)

¹Arizona State University, Tempe, Arizona 85287, USA

²National and Kapodistrian University of Athens, 15771 Athens, Greece

³Carnegie Mellon University, Pittsburgh, Pennsylvania 15213, USA

⁴The Catholic University of America, Washington, D.C. 20064, USA

⁵University of Connecticut, Storrs, Connecticut 06269, USA

⁶Florida International University, Miami, Florida 33199, USA

⁷Florida State University, Tallahassee, Florida 32306, USA

⁸The George Washington University, Washington, D.C. 20052, USA

⁹University of Glasgow, Glasgow G12 8QQ, United Kingdom

¹⁰GSI Helmholtzzentrum für Schwerionenforschung GmbH, D-64291 Darmstadt, Germany

¹¹Institute of High Energy Physics, Beijing 100049, People's Republic of China

¹²Indiana University, Bloomington, Indiana 47405, USA

¹³National Research Centre Kurchatov Institute, Institute for Theoretical and Experimental Physics, Moscow 117259, Russia

¹⁴Thomas Jefferson National Accelerator Facility, Newport News, Virginia 23606, USA

¹⁵University of Massachusetts, Amherst, Massachusetts 01003, USA

¹⁶Massachusetts Institute of Technology, Cambridge, Massachusetts 02139, USA

¹⁷National Research Nuclear University Moscow Engineering Physics Institute, Moscow 115409, Russia

¹⁸Norfolk State University, Norfolk, Virginia 23504, USA

¹⁹North Carolina A&T State University, Greensboro, North Carolina 27411, USA

²⁰University of North Carolina at Wilmington, Wilmington, North Carolina 28403, USA

²¹Northwestern University, Evanston, Illinois 60208, USA

²²Old Dominion University, Norfolk, Virginia 23529, USA

²³University of Regina, Regina, Saskatchewan, Canada S4S 0A2

²⁴Universidad Técnica Federico Santa María, Casilla 110-V Valparaíso, Chile

²⁵Tomsk State University, 634050 Tomsk, Russia

²⁶Tomsk Polytechnic University, 634050 Tomsk, Russia

²⁷A. I. Alikhanian National Science Laboratory (Yerevan Physics Institute), 0036 Yerevan, Armenia

²⁸College of William and Mary, Williamsburg, Virginia 23185, USA

²⁹Wuhan University, Wuhan, Hubei 430072, People's Republic of China

(Dated: September 12, 2019)

We report on the measurement of the $\gamma p \rightarrow J/\psi p$ cross section from $E_\gamma = 11.8$ GeV down to the threshold at 8.2 GeV using a tagged photon beam with the GlueX experiment. We find the total cross section falls toward the threshold less steeply than expected from two-gluon exchange models. The differential cross section $d\sigma/dt$ has an exponential slope of 1.67 ± 0.39 GeV⁻² at 10.7 GeV average energy. The LHCb pentaquark candidates P_c^+ can be produced in the s -channel of this reaction. We see no evidence for them and set model-dependent upper limits on their branching fractions $\mathcal{B}(P_c^+ \rightarrow J/\psi p)$ and cross sections $\sigma(\gamma p \rightarrow P_c^+) \times \mathcal{B}(P_c^+ \rightarrow J/\psi p)$.

INTRODUCTION

The exclusive production of charmonium near threshold provides a unique probe for studying the gluonic field in the nucleon and its dynamical coupling to the valence quarks. Recently, there has been increased interest in J/ψ photoproduction in the beam energy region of $E_\gamma = 9.4 - 10.1$ GeV, as it can be used to search for the pentaquark candidates reported by LHCb in the $J/\psi p$ channel of the $\Lambda_b^0 \rightarrow J/\psi p K^-$ decay [1, 2]. The LHCb collaboration initially claimed two pentaquark states, $P_c^+(4380)$ and $P_c^+(4450)$ [1]. Very recently, they reported the observation of three narrow pentaquark states, $P_c^+(4312)$, $P_c^+(4440)$, and $P_c^+(4457)$, where the previously reported $P_c^+(4450)$ was resolved into the latter two states with narrower widths [2]. In photoproduction, these resonances can be produced in the s -channel: $\gamma p \rightarrow P_c^+ \rightarrow J/\psi p$ [3–6], which is free from the three-body re-scattering effects proposed as one of the possible explanations of the structures observed by LHCb [7–9]. This reaction can be described by the $P_c^+ \rightarrow J/\psi p$ decay plus its time inversion, with the $J/\psi - \gamma$ coupling determined by Vector Meson Dominance (VMD) [10]. The Breit-Wigner cross section depends on the measured width of the pentaquark, the VMD coupling obtained from the leptonic decay of the J/ψ , and only one unknown parameter, the branching fraction of the $P_c^+ \rightarrow J/\psi p$ decay that enters quadratically. The pentaquarks produced in the s -channel would appear as structures in the J/ψ photoproduction cross section as a function of energy, possibly interfering with the non-resonant continuum. By measuring the resonant contribution one can estimate this branching fraction, which is complementary to the LHCb results.

A heavy quark system like the J/ψ interacts with the light quarks of the proton via gluon exchange. Close to threshold a large momentum is transferred to the proton ($|t| = 2.2$ GeV² at threshold). The energy dependence of the total cross section at high- t has been addressed within several approaches. Based on dimensional scaling rules, the energy dependence of the J/ψ photoproduction cross section was predicted with a dependence on the number of hard gluons involved in the reaction [11]. Near threshold all valence quarks of the proton are expected to participate in the reaction, requiring the involvement of three high- x gluons, while at higher energies one or two hard gluons can be involved. In Ref. [12], it is argued that the t -dependence of the exclusive reaction is defined by the proton gluonic form-factor, for which a dipole form is assumed in analogy with the electromagnetic form factors:

$$F(t) \propto 1/(1 - t/m_0^2)^2, \quad (1)$$

though with a different mass scale m_0 . The total cross section is proportional to the integral of $F^2(t)$ over a t -range that, near threshold, depends strongly on energy. According to Ref. [13], J/ψ photoproduction near threshold is dominated by the real part of the $J/\psi p$ elastic amplitude, which is of critical interest, since it contains the trace anomaly term related to the fraction of the nucleon mass arising from gluons. In Ref. [14] it was demonstrated that, in the near-threshold region, the shape of the cross section as a function of energy and t depends on the contribution of gluons to the nucleon mass.

In this Letter, we report on the first measurement of the cross section of the exclusive reaction $\gamma p \rightarrow J/\psi p$ from threshold up to $E_\gamma = 11.8$ GeV. We identify the J/ψ by its decay into an electron-positron pair. Previous measurements near threshold were inclusive and done on nuclear targets. The only published result in our energy region is at $E_\gamma \approx 11$ GeV, measured at Cornell [15]. Measurements at SLAC have been performed at photon beam energies of 13 GeV and above [16].

The data were collected by the GlueX experiment located in Hall D at Jefferson Lab during 2016 and 2017, representing about 25% of the total data accumulated by the experiment to date.

THE EXPERIMENT

The GlueX experiment uses a linearly-polarized, tagged photon beam produced by the 12 GeV Continuous Electron Beam Accelerator Facility (CEBAF). The electron beam is incident on a diamond radiator, and produces a bremsstrahlung spectrum proportional to $1/E_\gamma$ and a primary coherent peak adjusted to be in the energy range of 8.2 – 9.0 GeV. We also use data taken with an aluminum radiator, which does not produce coherent radiation. The scattered electron is analyzed with a 9 T-m dipole magnet and detected in a tagging scintillator array allowing the photon energy to be determined with a resolution of 0.2%. The photon beam is collimated through a 5 mm diameter hole at a distance of 75 m from the radiator. Following this, the photon flux and energy are monitored by an electron-positron pair spectrometer system [17].

The GlueX detector is based on a 2T, 4m-long solenoid magnet and has full azimuthal and $1^\circ < \theta < 120^\circ$ polar angle coverage. A 30cm-long liquid hydrogen target is placed inside the solenoid. A scintillating start counter surrounding

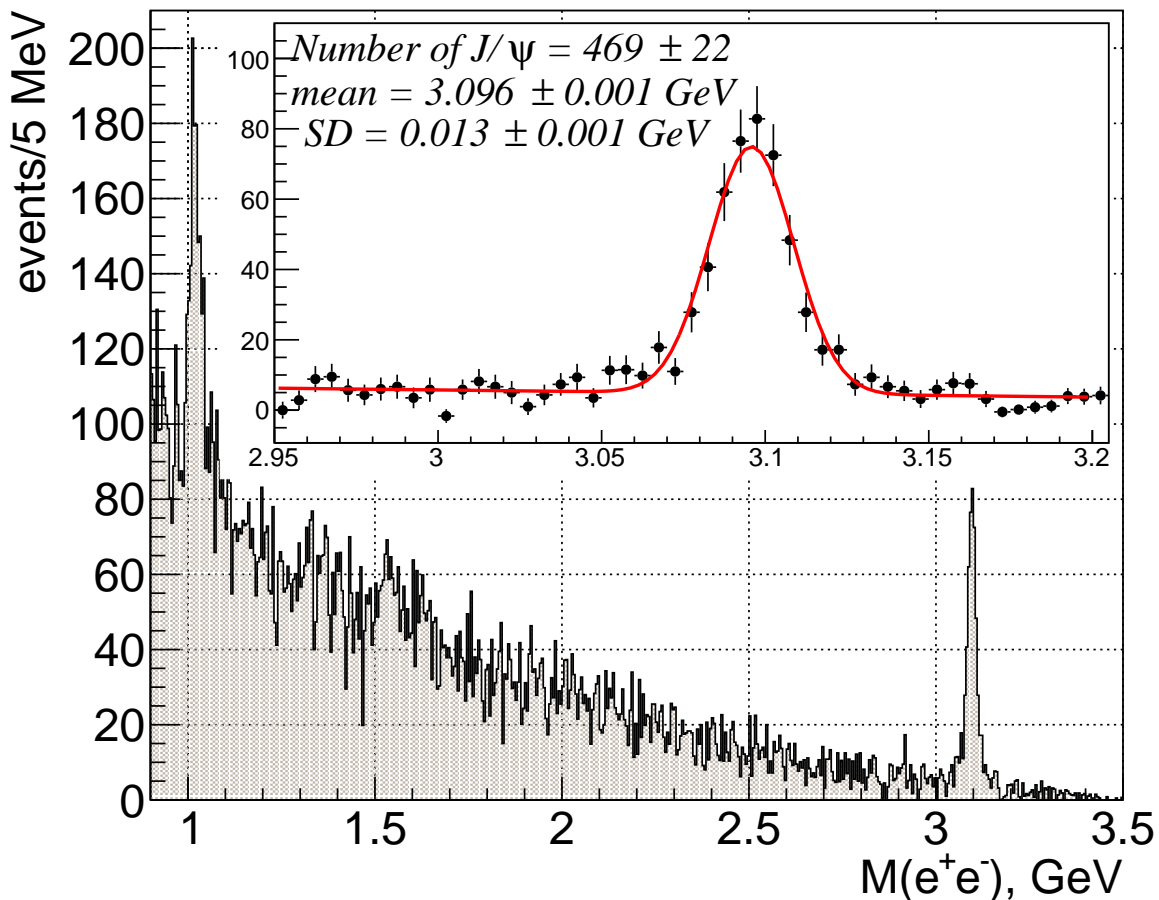


FIG. 1: Electron-positron invariant mass spectrum from the data. The insert shows the J/ψ region fitted with a linear polynomial plus a Gaussian (fit parameters shown).

the target helps to select the beam bunch [18]. Charged particle reconstruction around the target is performed by the Central Drift Chamber (CDC), consisting of straw tubes grouped in 28 layers with axial and stereo orientation. In the forward direction 24 planes of drift chambers with both wire and cathode strip readout are used [19]. The two drift chamber systems are surrounded by a lead-scintillator electromagnetic barrel calorimeter (BCAL) [20]. Electronically, the calorimeter is grouped in 192 azimuthal segments and in four radial layers, allowing the reconstruction of both transverse and longitudinal shower development.

The detector hermeticity in the forward direction outside of the magnet is achieved by the Time-of-Flight scintillator wall and the lead-glass electromagnetic Forward Calorimeter (FCAL), both located approximately 6 m from the target. Both calorimeters, FCAL and BCAL, are used to trigger the detector readout, requiring sufficient total energy deposition. The intensity of the beam in the region above the J/ψ threshold was 2×10^7 photons/s in 2016 and the first period of 2017, and was then increased to 5×10^7 photons/s for the rest of 2017, resulting in a total accumulated luminosity of ~ 68 pb $^{-1}$. In 2016 the maximum tagged photon energy was 11.85 GeV, while for 2017 it was lowered to 11.40 GeV. In 2017 the solenoid field was increased by 12% compared to 2016.

We study the exclusive reaction $\gamma p \rightarrow pe^+e^-$ in the region of the e^+e^- invariant mass $M(e^+e^-) > 0.90$ GeV, which includes the narrow ϕ and J/ψ peaks, and the continuum dominated by the Bethe-Heitler (BH) process. Figure 1 shows the $M(e^+e^-)$ spectrum data after applying the event selection criteria described below. We normalize the J/ψ total cross section to that of BH in the invariant mass range 1.20 – 2.50 GeV, thus canceling uncertainties from factors like luminosity and common detector efficiencies.

The electron/pion separation is achieved mainly by applying selections on p/E , where the charged particle momentum p comes from the kinematic fit described below, and E is the energy deposited in the calorimeters. We require

$-3\sigma < p/E - \langle p/E \rangle < +2\sigma$ for both lepton candidates, where the resolution σ of p/E for the sample of leptons in the BH region is 3.9% for FCAL and 6.8% for BCAL. We also take advantage of the radial layer structure of the BCAL, using the energy deposited in the innermost layer, E_{pre} , and requiring lepton candidates emitted at a polar angle θ to have $E_{pre}\sin\theta > 30$ MeV, taking into account the pathlength through the calorimeter. This rejects a significant number of pions, which deposit small amounts of energy in this layer compared to electrons. We require all charged particles to have momenta > 0.4 GeV and polar angle $> 2^\circ$ in order to reduce the contamination from the $\pi^+\pi^-p$ final state and poorly reconstructed events. Due to the steeper t -dependence of BH compared to $\pi^+\pi^-$ production, to minimize the pion background we select the BH process only in the low- t region, $-(t - t_{min}) < 0.6$ GeV².

Protons with momenta $\lesssim 1$ GeV are identified by their energy deposition in the CDC. The three final-state particles are required to be consistent in time with the same electron beam bunch (± 2 ns for most of the data). The tagged beam photons that are in time with this bunch qualify as possible candidates associated with the reaction. The contribution from beam photons accidental in time is subtracted statistically using a sample of photons that are out-of-time with respect to the reaction beam bunch.

Taking advantage of the exclusivity of the reaction and the relatively precise measurement of the beam energy, we use a kinematic fit to improve the resolution of the measured charged particle momenta. The fit enforces momentum and energy conservation and requires a common vertex for the three final-state particles. The electron-positron invariant mass spectrum in Fig. 1 is obtained using the results of the kinematic fit, which allows us to achieve a 13 MeV standard deviation (SD) mass resolution for the J/ψ . Studies of the kinematic fit show that the results are constrained primarily by the direction and magnitude of the proton momentum and the directions of the two leptons. In contrast to protons, the leptons are produced on average with higher momenta and smaller angles where the momenta are reconstructed with larger uncertainties. Therefore they do not affect the kinematic fit noticeably.

We extract the J/ψ and BH yields in bins of beam energy or t . The J/ψ yield is obtained by performing a binned likelihood fit to the invariant mass spectra, as in Fig. 1, with a Gaussian signal and linear background.

The reduction of the background in the BH region by more than three orders of magnitude after applying the electron/pion selections event-by-event is not enough to completely eliminate the pion contamination. On average the remaining sample contains 54% pions. To extract the BH yield we fit the peak and the pion background of the p/E distribution for one of the lepton candidates, while applying the p/E selection for the other candidate (see Supplemental Material).

We have performed Monte Carlo simulations of both J/ψ and continuum BH production. The BH diagrams can be calculated in QED. We have used two BH generators, one based on analytical calculations [21] and another [22] based on numerical calculations of the diagrams. We generate the J/ψ -proton final state using an exponential t -dependence and a cross section as a function of the beam energy obtained from our measurement, followed by the $J/\psi \rightarrow e^+e^-$ decay assuming helicity conservation.

The response of the GlueX detector to the generated events was simulated using GEANT3 [23]. Accidental tagger signals and detector noise signals were extracted from randomly triggered real data and injected into the generated events. We use these simulations to calculate the BH and J/ψ reconstruction efficiencies, ε_{BH} and $\varepsilon_{J/\psi}$. BH simulations are also used to integrate the BH cross section over the region used for normalization.

RESULTS AND DISCUSSION

We calculate the total cross section in 10 bins of beam energy using the following formula:

$$\sigma_{J/\psi}(E_\gamma) = \frac{N_{J/\psi}(E_\gamma)}{N_{BH}(E_\gamma)} \frac{\sigma_{BH}(E_\gamma)}{\mathcal{B}_{J/\psi}} \frac{\varepsilon_{BH}(E_\gamma)}{\varepsilon_{J/\psi}(E_\gamma)}. \quad (2)$$

Here $N_{J/\psi}$ and N_{BH} are the J/ψ and BH yields, σ_{BH} is the calculated BH cross section, and $\mathcal{B}_{J/\psi}$ is the $J/\psi \rightarrow e^+e^-$ branching ratio of 5.97% [24]. Note that the result depends on the relative BH to J/ψ efficiency. Effects due to variations in the photon flux over a given energy bin also cancel under the assumption that the J/ψ cross section varies slowly across a bin. The study of features in the J/ψ cross section that are narrower than an energy bin, such as those due to narrow pentaquarks, requires, in addition to the binned total cross sections, taking into account the finer flux structure.

We obtain results for the differential cross section in 7 bins of t integrated over the region $E_\gamma = 10.00 - 11.80$ GeV. For the normalization of the differential cross section we use the total BH yields instead of the yields in bins of t .

The total cross section in bins of beam energy and the differential cross section as a function of $-(t - t_{min})$, together with the statistical and systematic errors are given as Supplemental Material. We estimate the overall

normalization uncertainty to be 27%. The main contribution comes from the uncertainty in the relative BH to J/ψ efficiency determined from simulations, as the two processes occupy different kinematic regions. To test the accuracy of the simulations, we study the ratio of the measured BH cross section to the calculated one as a function of several kinematic variables, such as proton momentum and polar angle. Comparing these ratios obtained for the BH and J/ψ kinematic regions, we find the largest relative difference to be $(23 \pm 18)\%$ and take the central value to be the uncertainty due to this source.

The radiative correction to the J/ψ decay is simulated using the PHOTOS package [25]. The results show that the kinematic fit recovers the J/ψ electron-positron invariant mass to its value before radiation. This is expected because the dominant constraint to the fit is the recoil proton, which is decoupled from the J/ψ decay. This is not the case for the BH process, for which based on Ref. [26] we estimate 8.3% radiative correction in the extreme case, when the electron-positron invariant mass is not affected by the radiation, and only the proton is.

The maximum background contribution of the ρ' production to the e^+e^- continuum of 7% is estimated by comparing the results for two invariant mass ranges: 1.20 – 2.00 and 2.00 – 2.50 GeV. Based on Ref. [21] the contribution of Timelike Compton Scattering to the BH cross section is estimated to be less than 4%. Due to uncertainties of the Generalized Parton Distribution model used in this estimation, we double this value as a systematic uncertainty.

We assign the systematic uncertainties of the individual data points to the maximum deviations of the results obtained by varying the procedures for fitting the J/ψ peak in the e^+e^- invariant mass spectrum and the BH electron/positron peak in the p/E distribution. We assign the systematic error for the t -slope to the maximum deviation of the slope obtained with different J/ψ fitting methods. The uncertainties of the parameters used in the J/ψ simulations (t -slope, energy dependence) have a small effect.

As a cross-check, we have compared the total cross sections versus beam energy obtained from the 2016 and 2017 data sets, which represent different experimental conditions (solenoid field, photon beam intensity and spectrum). They are statistically consistent with an average ratio of 0.95 ± 0.14 . Based on the missing mass distribution, we set a 5% upper limit for the target excitation contribution, $\gamma p \rightarrow J/\psi p \pi^0$.

For the t -dependence of the differential cross section (see Supplemental Material) for beam energies of 10.00 – 11.80 GeV with an average of 10.72 GeV, we obtain an exponential t -slope of 1.67 ± 0.35 (stat.) ± 0.18 (syst.) GeV^{-2} . This can be compared with the Cornell result at $E_\gamma \approx 11$ GeV of 1.25 ± 0.20 GeV^{-2} [15] and the SLAC result at $E_\gamma = 19$ GeV of 2.9 ± 0.3 GeV^{-2} [16]. All these results are consistent [27] with the hypothesis in Ref. [12] of the dipole t -dependence for the differential cross section assuming a mass scale of 1.14 GeV, as given in Eq. (1).

The measured total cross section in bins of beam energy is shown in Fig. 2, and compared to the earlier measurements at Cornell [15] and SLAC [16]. Note that the SLAC experiment measured $d\sigma/dt$ at $t = t_{min}$. In order to estimate the total cross section, we have integrated over t assuming the dipole t -dependence with $m_0 = 1.14$ GeV.

Comparing the J/ψ cross section to the Brodsky *et al.* model [11], we find that our data do not favor either pure two- or three-hard-gluon exchange separately, and a combination of the two processes is required to fit the data adequately. Such a combination is shown in Fig. 2 assuming no interference between the two contributions. It appears that three-hard-gluon exchange dominates near threshold, consistent with the expectation that all the constituents should participate in the reaction.

The total cross section calculations of Kharzeev *et al.* [13] imply a large gluonic contribution to the nuclear mass and are shown in Fig. 2 multiplied by a factor 2.3. The shape of the curve agrees well with our measurements and the overall scale factor is within the claimed uncertainty of the calculation.

The narrow LHCb states, $P_c^+(4312)$, $P_c^+(4440)$, and $P_c^+(4457)$, produced in the s -channel would appear as structures at $E_\gamma = 9.44$, 10.04 and 10.12 GeV in the cross-section results shown in Fig. 2. We see no evidence for such structures. The initial report [1] claims the two states, $P_c^+(4380)$ and $P_c^+(4450)$, may have spin 3/2 or 5/2 with opposite parity. The spins/parities of the new states, $P_c^+(4312)$, $P_c^+(4440)$, and $P_c^+(4457)$, have not been determined yet. We evaluate the branching fraction limits $\mathcal{B}(P_c^+ \rightarrow J/\psi p)$ individually for each P_c assuming $J^P = 3/2^-$, with the lowest angular momentum $L = 0$ of the $J/\psi p$ system. As VMD leads to an increase in the cross section for increasing L [4], $L = 0$ minimizes the resulting cross section and therefore yields a maximal upper limit on the branching fraction. We fit our data, in which the statistical and systematic uncertainties on the individual points are added in quadrature, with a variation of the JPAC model [6] where the non-resonant component is described by a combination of Pomeron and tensor amplitudes [28]. To take into account the fine flux variations (see Supplemental Material), in each bin the data are fitted with the integral of the model function weighted by the normalized flux distribution across the extent of the bin. The upper limits on the branching fractions are determined by integrating the profile likelihood of the fit as a function of the branching fraction. The profile likelihood is determined by a procedure based on the one described in Ref. [29], in which uncertainties on the model parameters can be incorporated. As an example of the sensitivity of our measurement, we plot in Fig. 2 the model prediction for $P_c^+(4440)$ with $\mathcal{B}(P_c^+(4440) \rightarrow J/\psi p) = 1.6\%$, which is the estimated upper limit at 90% confidence level when taking into account the errors of the individual data points only.

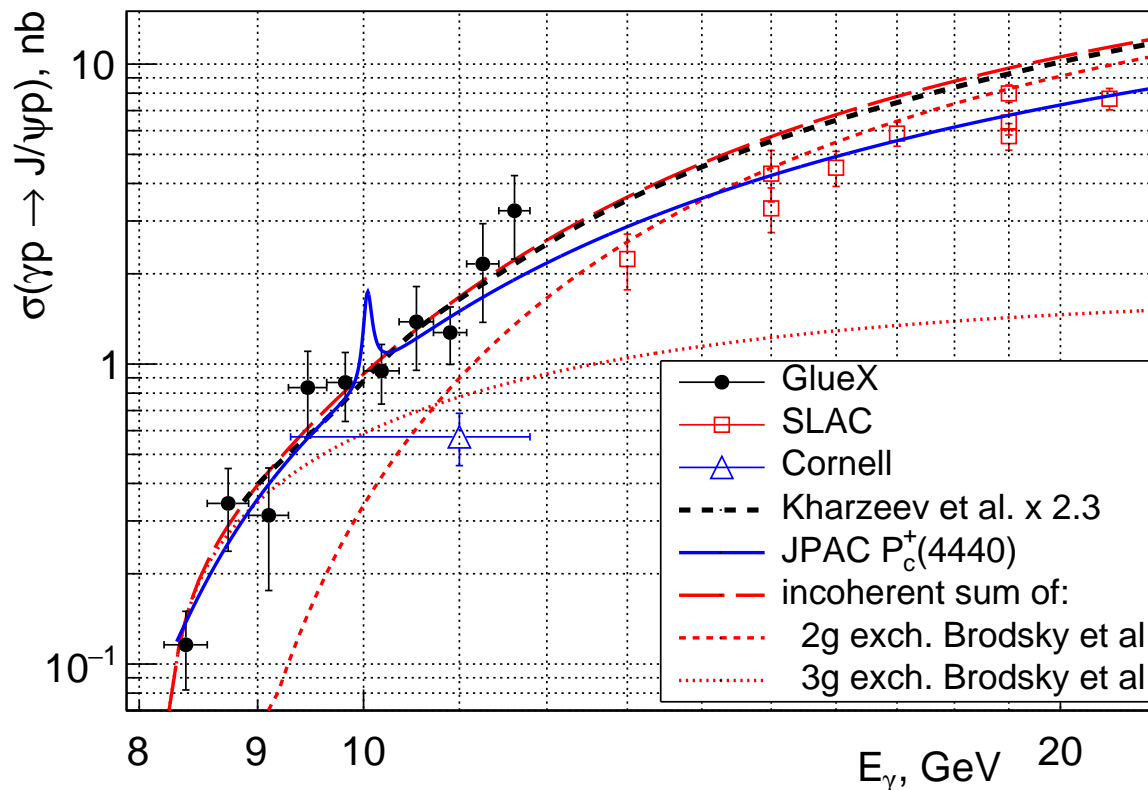


FIG. 2: J/ψ total cross section vs beam energy, compared to previous data [15, 16], theoretical predictions [11, 13], and JPAC model [6] for $\mathcal{B}(P_c^+(4440) \rightarrow J/\psi p) = 1.6\%$ and $J^P = 3/2^-$. All curves are fitted/scaled to the GlueX data only. For our data the quadratic sums of statistical and systematic errors are shown; the overall normalization uncertainty is 27%.

Similar curves for the other resonances are shown in the Supplemental Material. Including systematic uncertainties due to the non-resonant parametrization, Breit-Wigner parameters, and overall cross-section normalization, we determine upper limits at 90% confidence level of 4.6%, 2.3%, and 3.8% for $P_c^+(4312)$, $P_c^+(4440)$, and $P_c^+(4457)$, respectively. These upper limits become a factor of 5 smaller if $J^P = 5/2^+$ is assumed. Note that these results depend on the interference between the pentaquarks and the non-resonant continuum that is model dependent and the interference between the pentaquarks that is not taken into account.

A less model-dependent limit is found for the product of the cross section at the resonance maximum and the branching fraction, $\sigma_{max}(\gamma p \rightarrow P_c^+) \times \mathcal{B}(P_c^+ \rightarrow J/\psi p)$, using an incoherent sum of a Breit-Wigner and the non-resonant component of the model described above. Applying the same likelihood procedure that includes the systematic uncertainties, yields upper limits at 90% confidence level of 4.6, 1.8, and 3.9 nb for $P_c^+(4312)$, $P_c^+(4440)$, and $P_c^+(4457)$, respectively.

In Refs. [30–32] the partial widths of the $P_c^+ \rightarrow J/\psi p$ decays were calculated and shown to be orders of magnitude different for two pentaquark models, the hadrocharmonium and molecular models. Our upper limits on the branching fractions do not exclude the molecular model, but are an order of magnitude lower than the predictions in the hadrocharmonium scenario.

In summary, we have made the first measurement of the J/ψ exclusive photoproduction cross section from $E_\gamma = 11.8$ GeV down to the threshold, which provides important inputs to models of the gluonic structure of the proton at high x . The measured cross section is used to set model-dependent upper limits on the branching fraction of the LHCb P_c^+ states, which allow to discriminate between different pentaquark models.

We would like to acknowledge the outstanding efforts of the staff of the Accelerator and the Physics Divisions at Jefferson Lab that made the experiment possible. This work was supported in part by the U.S. Department of Energy, the U.S. National Science Foundation, the German Research Foundation, GSI Helmholtzzentrum für Schwerionen-

forschung GmbH, the Natural Sciences and Engineering Research Council of Canada, the Russian Foundation for Basic Research, the UK Science and Technology Facilities Council, the Chilean Comisión Nacional de Investigación Científica y Tecnológica, the National Natural Science Foundation of China and the China Scholarship Council. This material is based upon work supported by the U.S. Department of Energy, Office of Science, Office of Nuclear Physics under contract DE-AC05-06OR23177. S. Dobbs acknowledges the support of Jefferson Science Associates, LLC.

* Corresponding author: pentchev@jlab.org

- [1] R. Aaij *et al.* (LHCb Collaboration), Phys. Rev. Lett. **115**, 072001 (2015).
- [2] R. Aaij *et al.* (LHCb Collaboration), Phys. Rev. Lett. **122**, 222001 (2019).
- [3] Q. Wang, X.-H. Liu, and Q. Zhao, Phys. Rev. D **92**, 034022 (2015).
- [4] V. Kubarovsky and M. B. Voloshin, Phys. Rev. D **92**, 031502 (2015).
- [5] M. Karliner and J. Rosner, Phys. Lett. B **752**, 329 (2016).
- [6] A. Blin, C. Fernandez - Ramirez, A. Jackura, V. Mathieu, V. Mokeev, A. Pilloni, and A. Szczepaniak, Phys. Rev. D **94**, 034002 (2016).
- [7] F.-K. Guo, U.-G. Meißner, W. Wang, and Z. Yang, Phys. Rev. D **92**, 071502 (2015).
- [8] X. H. Liu, Q. Wang, and Q. Zhao, Phys. Lett. B **757**, 231 (2016).
- [9] M. Mikhasenko, arXiv:1507.06552 (2015).
- [10] The possible limitations of the VMD for heavy quark mesons are discussed in Ref. [4].
- [11] S. Brodsky, E. Chudakov, P. Hoyer, and J. Laget, Phys. Lett. B **498**, 23 (2001).
- [12] L. Frankfurt and M. Strikman, Phys. Rev. D **66**, 031502 (2002).
- [13] D. Kharzeev, H. Satz, A. Syantomov, and G. Zinovev, Nucl.Phys. A **661**, 568 (1999).
- [14] Y. Hatta and D.-L. Yang, Phys. Rev. D **98**, 074003 (2018).
- [15] B. Gittelman, K. M. Hanson, D. Larson, E. Loh, A. Silverman, and G. Theodosiou, Phys. Rev. Lett. **35**, 1616 (1975).
- [16] U. Camerini, J. Learned, R. Prepost, C. Spencer, D. Wisner, W. Ash, R. L. Anderson, D. M. Ritson, D. Sherden, and C. K. Sinclair, Phys. Rev. Lett. **35**, 483 (1975).
- [17] F. Barbosa, C. Hutton, A. Sitnikov, A. Somov, S. Somov, and I. Tolstukhin, Nucl. Instrum. Meth. A **795**, 376 (2015).
- [18] E. Pooser, F. Barbosa, W. Boeglin, C. Hutton, M. Ito, M. Kamel, P. K. A. LLodra, N. Sandoval, S. Taylor, T. Whitlatch, S. Worthington, C. Yero, and B. Zihlmann, Nucl. Instrum. Meth. A **927**, 330 (2019).
- [19] L. Pentchev, F. Barbosa, V. Berdnikov, D. Butler, S. Furlotov, L. Robison, and B. Zihlmann, Nucl. Instrum. Meth. A **845**, 281 (2017).
- [20] T. D. Beattie, A. M. Foda, C. L. Henschel, S. Katsaganis, S. T. Krueger, G. J. Lolos, Z. Papandreou, *et al.*, Nucl. Instrum. Meth. A **896**, 24 (2018).
- [21] E. Berger, M. Diehl, and B. Pire, Eur.Phys.J.C **23**, 675 (2002).
- [22] R. Jones, Numerical calculations of the tree level QED diagrams using Diracxx package: <https://github.com/rjones30/Diracxx>.
- [23] R. Brun *et al.*, Report No. CERN-DD-78-2-REV (1978).
- [24] M. Tanabashi *et al.*, Phys. Rev. D **98**, 030001 (2018).
- [25] E. Barberio *et al.*, Comput. Phys. Commun. **79**, 291 (1994).
- [26] M. Heller, O. Tomalak, and M. Vanderhaeghen, Phys. Rev. D **97**, 076012 (2018).
- [27] L. Pentchev (for the GlueX collaboration), accepted for publication in JPS Conference Proceedings of the 8th International Conference on Quarks and Nuclear Physics (2019).
- [28] V. Mathieu, private communication (2018).
- [29] W. A. Rolke, A. M. Lopez, and J. Conrad, Nucl. Instrum. Meth. A **551**, 493 (2005).
- [30] M. I. Eides, V. Yu. Petrov, and M. V. Polyakov, Eur. Phys. J. **C78**, 36 (2018).
- [31] M. I. Eides and V. Yu. Petrov, Phys. Rev. **D98**, 114037 (2018).
- [32] M. I. Eides, V. Y. Petrov, and M. V. Polyakov, arXiv:1904.11616 (2019).

First measurement of near-threshold J/ψ exclusive photoproduction off the proton: Supplemental Material

The total cross-section in bins of beam energy and the differential cross-section as function of $-(t - t_{min})$ are given in Tables I and II together with the statistical and systematic errors for the individual data points. Table III summarizes our estimate of the systematic errors for the overall cross-section normalization.

Energy bin, GeV	σ , nb	stat. error, nb	syst. error, nb
8.2-8.56	0.116	0.031	0.013
8.56-8.92	0.343	0.067	0.082
8.92-9.28	0.313	0.127	0.052
9.28-9.64	0.835	0.194	0.185
9.64-10	0.868	0.196	0.109
10-10.36	0.949	0.187	0.102
10.36-10.72	1.383	0.284	0.323
10.72-11.08	1.274	0.206	0.184
11.08-11.44	2.158	0.421	0.657
11.44-11.8	3.245	0.928	0.384

TABLE I: $\gamma p \rightarrow J/\psi p$ total cross-sections, statistical and systematic errors of the individual points in bins of beam energy.

$-(t - t_{min})$ bin, GeV ²	$d\sigma/dt$, nb/GeV ²	stat. error, nb/GeV ²	syst. error, nb/GeV ²
0-0.15	1.643	0.334	0.058
0.15-0.3	1.249	0.265	0.019
0.3-0.45	1.088	0.248	0.012
0.45-0.6	0.627	0.182	0.024
0.6-0.75	0.599	0.163	0.047
0.75-0.9	0.470	0.145	0.006
0.9-1.05	0.400	0.134	0.011

TABLE II: Differential cross-sections, statistical and systematic errors of the individual points in bins of $-(t - t_{min})$.

Origin	Estimate, %
$\varepsilon_{BH}/\varepsilon_{J/\psi}$ relative efficiency	23
Radiative corrections	8.3
TCS contribution to BH	8
ρ' contribution to BH	7
total	26.7

TABLE III: Contributions to the total normalization error added quadratically.

The total cross-section calculated from the SLAC [16] data and shown in Fig. 2 of the paper is given in Table IV.

In Fig. 3 we show the GlueX result for the t -dependence of the differential cross section (exponential t -slope shown) for beam energies of 10.00 – 11.80 GeV with an average of 10.72 GeV. Closer to threshold, due to the strong variation of t_{min} and the smaller t -range, such an analysis requires slices in beam energy for which we do not have sufficient statistics.

Energy , GeV	σ , nb	error, nb
13	2.240	0.472
15	3.304	0.560
15	4.312	0.840
16	4.515	0.606
17	5.866	0.543
19	5.750	0.586
19	6.389	0.586
19	7.986	0.532
21	7.667	0.630

TABLE IV: Total cross-section vs beam energy calculated from $d\sigma/dt$ (at $t = t_{min}$) from the SLAC data [16] assuming dipole t -dependence, Eq.(1) $m_0 = 1.14$ GeV in the paper.

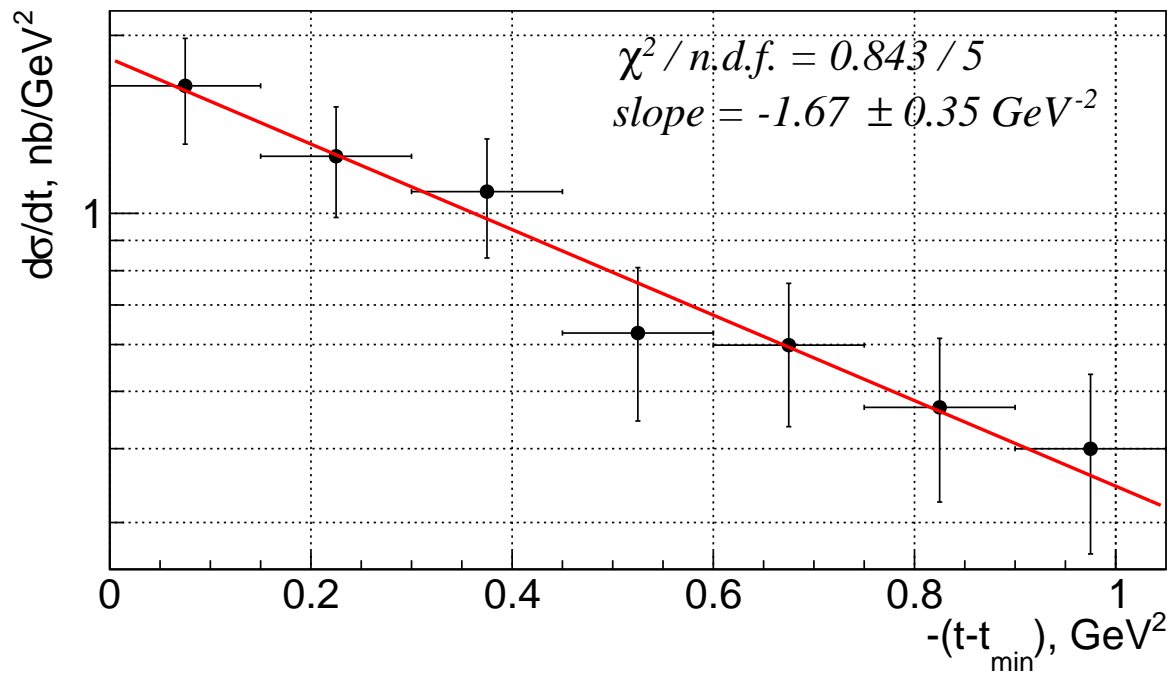


FIG. 3: Differential cross section for J/ψ photoproduction as a function of $-(t - t_{min})$ for $10.00 < E_\gamma < 11.80$ GeV.

In Fig. 4 the GlueX, SLAC, and Cornell results for the total cross-section are compared to the JPAC model curves for the three LHCb pentaquarks separately with branching fractions corresponding to the upper limits as estimated in the paper, when using only the errors of the individual data points.

The results for the upper limits of the pentaquark branching fractions $\mathcal{B}(P_c^+ \rightarrow J/\psi p)$ are summarized in Table V.

The tagged GlueX beam energy spectrum, given as an accumulated luminosity, is shown in Fig. 5. It is a result of using both, diamond (dominantly) and amorphous radiators.

The procedure for extracting the electron/positron BH yield is illustrated in Figs. 6,7. It is applied separately for the two calorimeters (BCAL and FCAL) and in bins of beam energy in order to obtain the final cross section results. The pion contamination varies between between 30 and 60%.

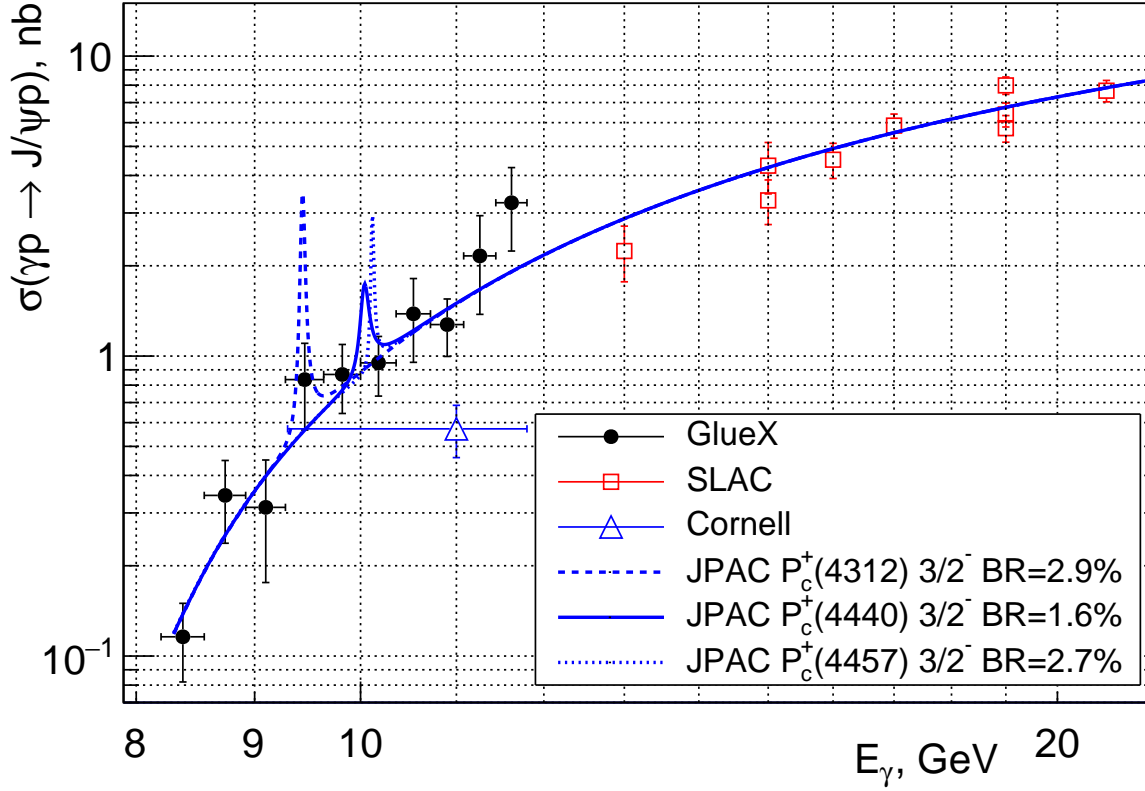


FIG. 4: GlueX results for the J/ψ total cross-section vs beam energy, Cornell [15], and SLAC [16] data compared to the JPAC model [6] corresponding to $\mathcal{B}(P_c^+(4312) \rightarrow J/\psi p) = 2.9\%$, $\mathcal{B}(P_c^+(4440) \rightarrow J/\psi p) = 1.6\%$, and $\mathcal{B}(P_c^+(4457) \rightarrow J/\psi p) = 2.7\%$, for the $J^P = 3/2^-$ case as discussed in the paper.

	$\mathcal{B}(P_c^+ \rightarrow J/\psi p)$ Upper Limits, %		$\sigma_{\max} \times \mathcal{B}(P_c^+ \rightarrow J/\psi p)$ Upper Limits, nb	
	p.t.p. only	total	p.t.p. only	total
$P_c^+(4312)$	2.9	4.6	3.7	4.6
$P_c^+(4440)$	1.6	2.3	1.2	1.8
$P_c^+(4457)$	2.7	3.8	2.9	3.9

TABLE V: Summary of the estimated upper limits for the P_c^+ states at 90% confidence level, as discussed in the paper. Separately shown are the results when using the errors of the individual data points (p.t.p.) only and the total ones that include the uncertainties in the model parameters and the overall normalization.

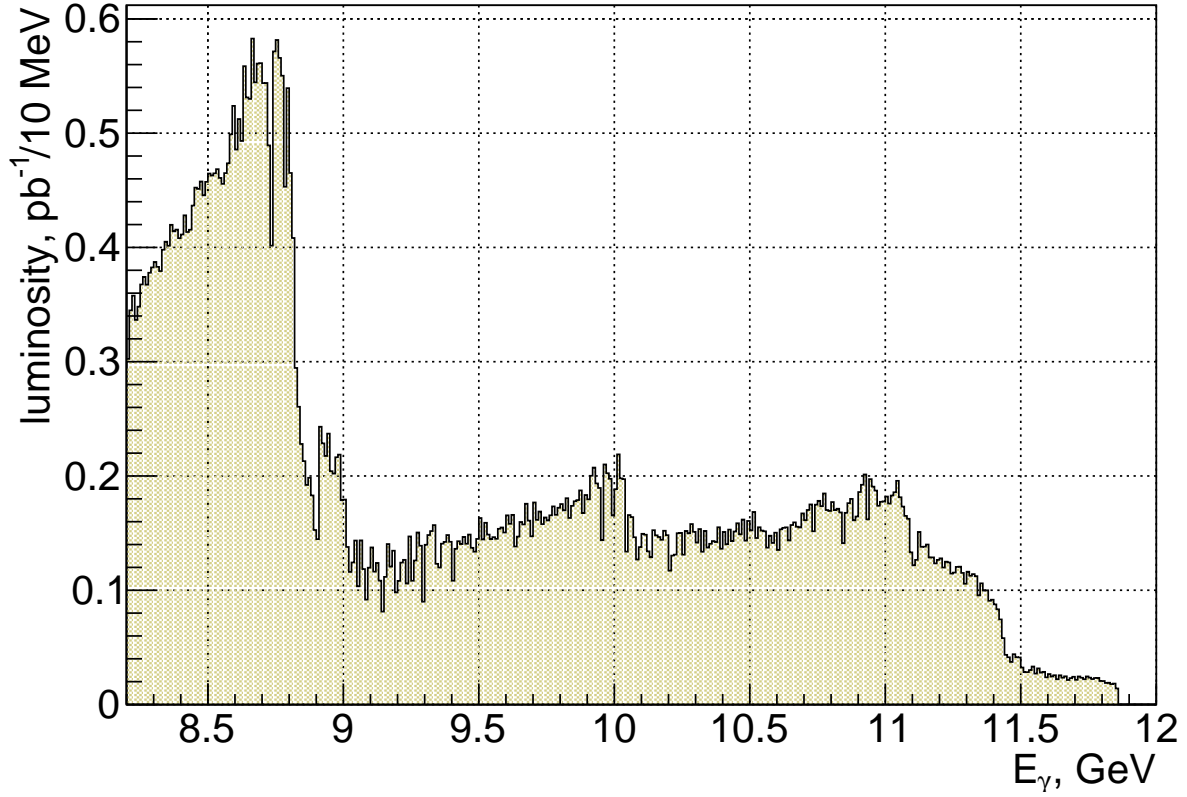


FIG. 5: The tagged photon luminosity as a function of beam energy.

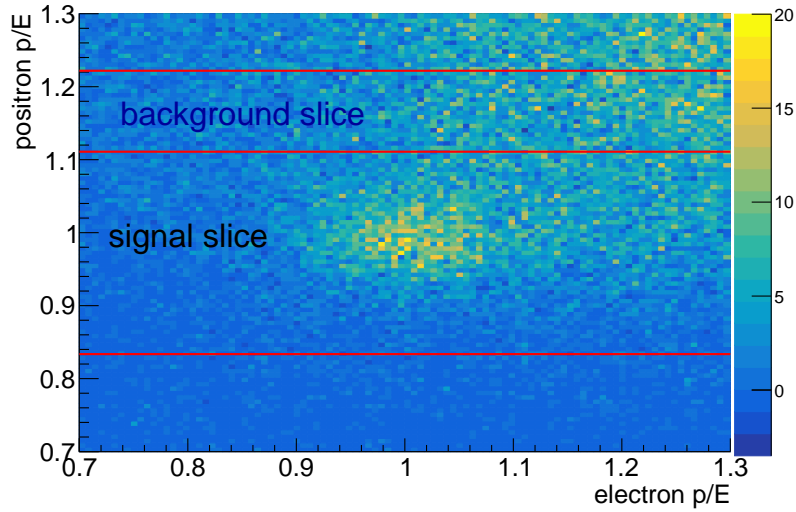


FIG. 6: p/E distribution of the two leptons. The background slice ($2\sigma < p/E - 1 < 4\sigma$ cut on the y-axis), and the slice containing the signal ($-3\sigma < p/E - 1 < 2\sigma$ cut on the y-axis) are indicated with horizontal lines.

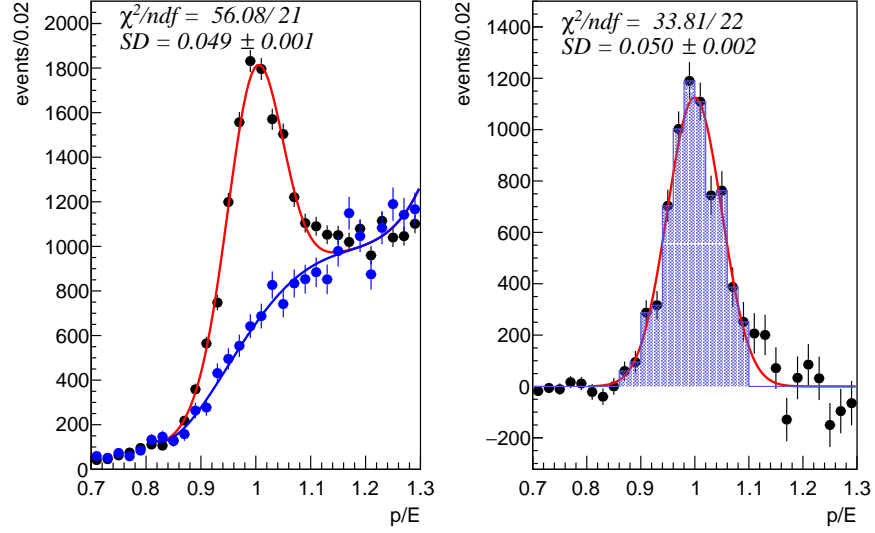


FIG. 7: Left plot: the signal slice from Fig.6 projected on the x-axis (black points) fitted with a background shape times a normalization parameter p_{norm} (blue line) plus a Gaussian (red line); the background shape is a polynomial fit of the projection of the background slice from Fig.6 (blue points normalized by p_{norm}). Right plot: the difference of the black and blue points from the left plot representing the electron/positron signal fitted with a Gaussian. The BH yield is assigned to the number of events within $(-3\sigma, +2\sigma)$ of the peak (shaded histogram).